

# Morphology, Mechanical and Viscoelastic Properties of Nitrile Rubber/Epoxidized Natural Rubber Blends

Asha Elizabeth Mathai, Sabu Thomas

School of Chemical Sciences, Mahatma Gandhi University, Priyadarshini Hills P.O., Kottayam, Kerala, 686560, India

Received 9 October 2003; accepted 11 May 2004

DOI 10.1002/app.21480

Published online in Wiley InterScience (www.interscience.wiley.com).

**ABSTRACT:** A new class of blend membranes from blends of nitrile rubber (NBR) and epoxidized natural rubber (ENR) has been prepared and their morphology, miscibility, mechanical, and viscoelastic properties have been studied. The ebonite method was used to study the blend morphology of the membranes. The morphology of the blends indicated a two-phase structure in which the minor phase is dispersed as domains in the major continuous phase. The performance of NBR/ENR blend membranes has been studied from the mechanical measurements. The viscoelastic behavior of the blends has been analyzed from the dynamic mechanical data. An attempt was made to relate

the viscoelastic behavior with the morphology of the blends. Various composite models have been used to predict the experimental viscoelastic data. The area under the linear loss modulus curve was larger than that obtained by theoretical group contribution analysis. The homogeneity of the system was further evaluated by Cole–Cole analysis. Finally, a master curve for the modulus of the blend was generated by applying the time–temperature superposition principle. © 2005 Wiley Periodicals, Inc. *J Appl Polym Sci* 97: 1561–1573, 2005

**Key words:** nitrile rubber; epoxidized natural rubber; miscibility; morphology; mechanical properties

## INTRODUCTION

The objective of polymer blending is to achieve commercially viable products having unique properties or low cost.<sup>1</sup> Although blending is a very simple technique, many of the polymer pairs are immiscible and incompatible. This leads to poor mechanical properties. The most important polymeric properties related to rubber/rubber blends are homogeneity of mixing and cure compatibility. Homogeneity at a microscopic level is necessary for optimum performance, but some degree of microheterogeneity is usually desirable to preserve the individual properties of the respective polymer components. Even though true miscibility may not be required, adhesion between polymer phases is necessary for good properties.

The morphology of a blend is a function of the nature of the blend components (both their mutual compatibility and the rheological properties of the components) and of the method employed to produce the blend. The blend morphology is strongly affected by composition, interfacial tension, and viscosity ratio. For the same processing condition, the blend morphology is reported to be determined by the composition ratio and melt viscosity difference of the components.<sup>2</sup> Continuity of a phase is favored by high volume frac-

tion and low viscosity relative to that of the other component. A blend morphology wherein one component is dispersed within a continuum of the other has received great attention in the literature. Dao<sup>3</sup> reported that the properties of polymer blends are strongly influenced by the morphology of the system. Cimmino et al.<sup>4</sup> studied the relationship between the mechanical properties of binary polyamide 6/rubber blends and their morphology. Recently, Thomas and co-workers<sup>5–10</sup> investigated the morphology of many polymer blends.

For investigating the structure–property relations and viscoelastic behavior of polymeric materials, dynamic mechanical test methods are widely used. The dynamic properties of polymeric materials are of considerable practical significance for several reasons, particularly if they are determined over a wide range of frequency and temperature. They can give insight into various aspects of material structure besides being a convenient measure of polymer transition temperatures. From dynamic mechanical studies, Ramesh and De<sup>11</sup> reported that an immiscible composition of polyvinyl chloride (PVC)/epoxidized natural rubber (ENR) blend becomes progressively miscible by the addition of carboxylated nitrile rubber (XNBR). Varughese et al.<sup>12</sup> studied the miscibility of PVC with 50% epoxidized natural rubber using DMA. Synthesis and properties of sequential interpenetrating polymer networks based on NBR and polyvinyl acetate were investigated by Patri et al.<sup>13</sup> by using tensile test, DSC, DMA, and swelling measurements. The viscoelastic

Correspondence to: S. Thomas (sabut552001@yahoo.com or sabuthom@satyam.net.in).

TABLE I  
Details of Materials Used

Materials	Characteristics	Source
Nitrile rubber (Aparene N553 NS)	Volatile matter (%)	0.130
	Antioxidant (%)	1.400
	Organic acid (%)	0.250
	Soap (%)	0.004
	Mooney viscosity (ML <sub>1+4</sub> 100°C)	40.000
	Bound acrylonitrile (%)	34.000
	Intrinsic viscosity (dl/g)	1.527
Epoxidized natural rubber (Epoxyprrene)	Epoxidation level (%)	50 ± 2
	Glass transition temperature (°C)	-24
	Density (kg/m <sup>3</sup> )	1.02
	Solubility parameter (Jm <sup>-3</sup> ) <sup>12</sup>	18.2
	Number average mol wt ( $\bar{M}_n$ )	9.9 × 10 <sup>5</sup>
	Gel content (%)	79 ± 3

behavior of many polymer blends has been studied earlier by our research group.<sup>14-18</sup>

Nitrile rubber is a unique synthetic elastomer, well known for its oil- and fuel- resistant behavior and its use in a variety of applications like oil seals, gaskets, etc. Epoxidized natural rubber is a versatile elastomer, noted for its ability to strain crystallize and its high glass transition temperature. ENR vulcanizates exhibit low gas permeability, high oil resistance, and high tensile, fatigue, or tear strength. The blending of NBR with epoxidized natural rubber is beneficial where the properties of NBR are required in combination with high tensile, fatigue, or tear strengths, particularly when the use of reinforcing fillers is not practical. To our knowledge, no serious attempt has been made so far, to evaluate the morphology and properties of these blends. The main objective of the present study is a detailed investigation of morphology, miscibility, mechanical, and viscoelastic behavior of nitrile rubber/ epoxidized natural rubber blends.

## EXPERIMENTAL PROCEDURES

### Materials

Nitrile rubber (Aparene-N 553 NS) with a bound acrylonitrile content of 34%, was supplied by Gujarat Apar Polymers Ltd, Mumbai, India. Epoxidized natural rubber epoxyprrene with 50 mol % epoxidation (ENR-50) was supplied by Rubber Research Institute, Malaysia. The basic characteristics of the materials are shown in Table I. All the rubber chemicals were of commercial grade. The mixing was done on a two-roll mixing mill (friction ratio 1 : 1.4) and vulcanizing agents were incorporated as per ASTM procedure. The basic formulation used is given in Table II. Nitrile rubber/ epoxidized natural rubber blend membranes were prepared by the masterbatch technique. The blend compositions are denoted by E<sub>0</sub>, E<sub>30</sub>, E<sub>50</sub>, E<sub>70</sub>,

and E<sub>100</sub>, where the subscripts denote the weight percentage of ENR in the blend. The cure characteristics of the mixes were determined on a Goettfert Elastograph (Goettfert, 67.5, Rev. 1.5, Germany) at 150°C. The compounds were then compression molded along the mill grain direction using an electrically heated hydraulic press at 150°C.

### Morphology

Morphology of elastomer blends can be studied by the ebonite method in which the preferential reaction of one of the rubber phases with sulfur and zinc oxide effects a large increase in its electron density.<sup>19</sup> Small rubber specimens were immersed in a molten mixture of a 90 : 5 : 5 weight ratio of sulfur, a sulphenamide accelerator (*N*-cyclo hexyl-2- benzo thiazyl sulphenamide), and zinc stearate for about 8 h at 120°C. The excess sulfur was carefully scraped off from the outer

TABLE II  
Compounding Recipe (Parts per Hundred Parts of Rubber by Weight)

Ingredients	ENR-50	NBR
ZnO	5.0	5.0
Stearic acid	2.0	1.0
Na <sub>2</sub> CO <sub>3</sub>	0.3	-
Sulphur	0.3	0.5
TDQ <sup>a</sup>	2.0	-
MBTS <sup>b</sup>	2.4	-
TMTD <sup>c</sup>	1.6	1.5
CBS <sup>d</sup>	-	1.5
PVI <sup>e</sup>	0.2	-

<sup>a</sup> Trimethyl dihydro quinoline.

<sup>b</sup> Dibenzothiazole disulphide.

<sup>c</sup> Tetra methyl thiuram disulphide.

<sup>d</sup> *N*-cyclohexyl-2-benzothiazole sulphenamide.

<sup>e</sup> Prevulcanization inhibitor (*N*-(cyclohexylthio)phthalimide).

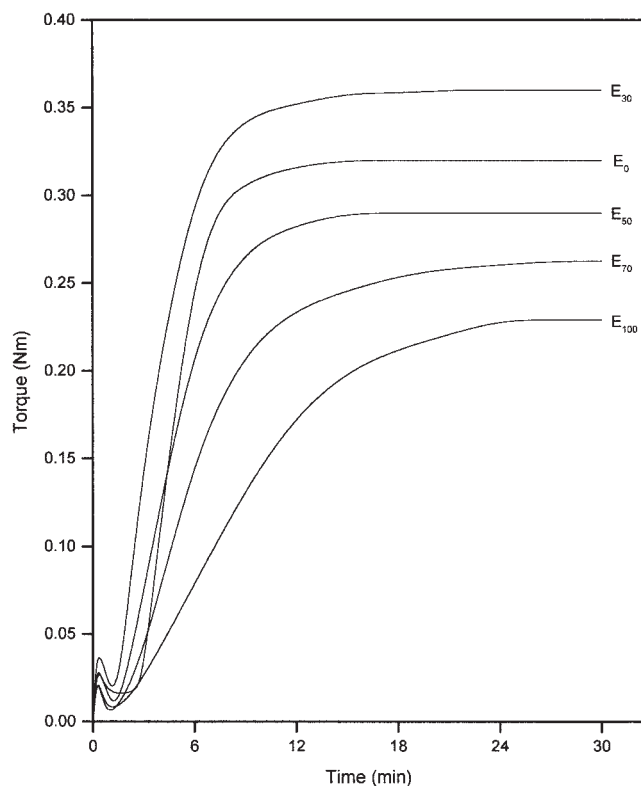


Figure 1 Elastographs of NBR/ENR blends.

surface before thin sections were cut for SEM observations using a Phillips (Netherlands) model scanning electron microscope operating at 10 kV. The dimensions of the dispersed phase were calculated from the SEM photomicrographs by considering more than 300 domains.

### Mechanical properties

Tensile testing of the samples was done at 25°C according to ASTM D 412-98 test method using dumb bell-shaped test pieces at a crosshead speed of 500 mm/min using a Universal Testing Machine, TNE Series 9200.

### Dynamic mechanical analysis

The dynamic mechanical properties of the blends were measured using a Polymer Laboratories (MK III) viscoelasticmeter. Compression molded samples of dimensions  $5 \times 0.5 \times 0.05 \text{ cm}^3$  were used for testing. The temperature range used was from  $-70$  to  $30^\circ\text{C}$ .

## RESULTS AND DISCUSSION

### Cure characteristics

The elastographs of the mixes are given in Figure 1 and cure characteristics are given in Table 3. In the

rheograph, torque is plotted against time. The minimum torque in the rheograph is presented as minimum viscosity value ( $M_L$ ) and is a measure of the extent of mastication. The lowest value of  $E_{100}$  indicates its higher extent of mastication during mixing. The maximum torque in the rheograph is presented as maximum viscosity. The highest value is for  $E_{30}$  composition. From the formulations it can be seen that in the present study the membranes were vulcanized with the efficient vulcanizing (EV) system. In the efficient vulcanizing system, the high accelerator/sulfur ratio results in shorter crosslinks, predominantly of the mono or disulfidic type.

The rheometric scorch time  $t_2$ , (premature vulcanization time) is the time taken for minimum torque value to increase by two units. The  $E_0$  composition shows maximum scorch safety. Optimum cure time ( $t_{90}$ ) is the vulcanization time to get optimum physical properties and it is the time corresponding to optimum cure torque.  $E_{100}$  shows maximum cure time while  $E_{30}$  composition shows minimum cure time. The cure rate index (CRI) is calculated using the equation

$$CRI = 100/t_{90} - t_2 \quad (1)$$

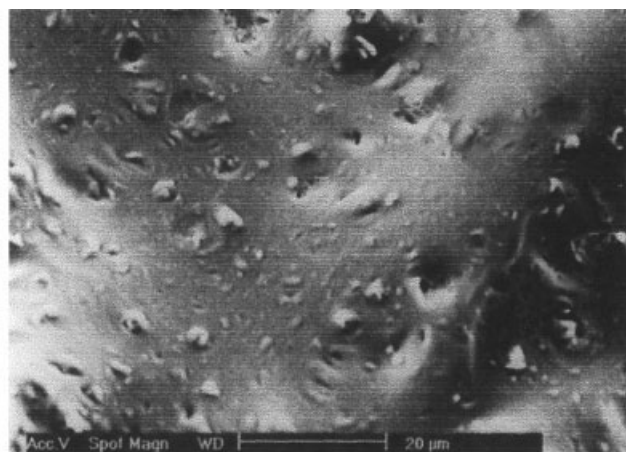
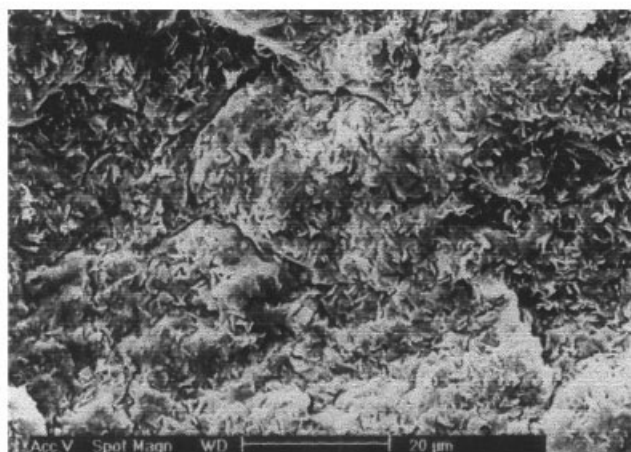
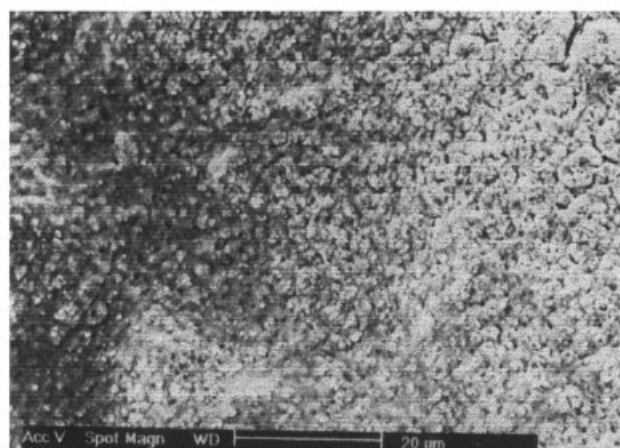
The higher the CRI values the higher the vulcanization rate. From Table III it can be seen that NBR has the highest cure rate and ENR has the minimum. Among the blend compositions,  $E_{30}$  has the highest cure rate. The high CRI value of NBR is due to its high degree of unsaturation.

### Morphology of the blend membranes

The polymer blend properties are strongly influenced by the morphology of the system. The SEM photographs of different blend membranes are shown in Figure 2(a-c). The tiny holes observed in the figure come from the debonding of the dispersed phase from the continuous phase. During mixing, the dispersed domains of the rubber blends are deformed while passing through the high shear regions of the mixing mill and it undergoes fracture to produce smaller particles or coalesces to form larger dispersed domains.<sup>20</sup> Figure 3 shows a schematic model of morphology

TABLE III  
Cure Characteristics of NBR/ENR Blends

Cure characteristics	$E_{100}$	$E_{70}$	$E_{50}$	$E_{30}$	$E_0$
Minimum torque (Nm)	0.007	0.005	0.010	0.016	0.015
Maximum torque (Nm)	0.23	0.26	0.29	0.36	0.32
Scorch time (min)	1.77	1.78	1.79	1.81	3.75
Optimum cure time (min)	17.75	12.20	8.72	7.36	7.60
CRI ( $\text{min}^{-1}$ )	6.26	9.60	14.41	18.01	25.97

20.0 kV 5.0 1000x 8.4 E<sub>30</sub> (a)20.0 kV 5.0 1000x 9.4 E<sub>50</sub> (b)20.0 kV 5.0 1000x 9.5 E<sub>70</sub> ©

**Figure 2** Scanning electron micrographs of NBR/ENR blends (a) E<sub>30</sub>, (b) E<sub>50</sub>, and (c) E<sub>70</sub>.

development in polymer blends.<sup>21</sup> A large piece of the dispersed phase is dragged across a hot surface to form a large number of sheets or ribbons of the dis-

persed phase in the matrix. Due to the effects of interfacial tension these sheets are unstable and holes begin to form in them. When the holes in the sheet or ribbon attain a sufficient size and concentration, a lace structure is formed, which begins to break apart due to shearing and interfacial forces into irregularly shaped pieces. These pieces are approximately the diameter of the particles, which are generated in the blend at long mixing times. These irregular pieces continue to break down under the action of shear and interfacial forces until all of the particles become nearly spherical. The blend morphology obtained represents the competition between the break up of the rubber particles and their flow-induced coalescence. The presented morphologies are proof of this behavior in NBR/ENR blends. In E<sub>30</sub> and E<sub>70</sub>, the minor phase is dispersed in the major continuous phase. The E<sub>50</sub> composition shows a co-continuous morphology, where both the phases are continuous. The size characteristics of the dispersed phase ( $\bar{D}_n$ ,  $\bar{D}_w$ ,  $\bar{D}_a$ , and  $\bar{D}_v$ ) and its distribution (poly dispersity index values) in the different blend compositions are presented in Table IV. These are calculated using the equations<sup>22</sup>

Number average diameter

$$\bar{D}_n = \frac{\sum N_i D_i}{\sum N_i} \quad (2)$$

Weight average diameter

$$\bar{D}_w = \frac{\sum N_i D_i^2}{\sum N_i D_i} \quad (3)$$

Surface area average diameter

$$\bar{D}_a = \sqrt{\frac{\sum N_i D_i^2}{\sum N_i}} \quad (4)$$

Volume average diameter

$$\bar{D}_v = \frac{\sum N_i D_i^4}{\sum N_i D_i^3} \quad (5)$$

where  $N_i$  is the number of particles having a diameter  $D_i$ . The domain size measurements were done by image analysis. A large number of domains (> 300) were considered for diameter measurements.

The poly dispersity index (PDI), which is a direct measure of size distribution of the dispersed phase, is calculated as

$$PDI = \bar{D}_w / \bar{D}_n \quad (6)$$

In NBR/ENR blends it is clear from the table that the values of  $\bar{D}_n$ ,  $\bar{D}_a$ ,  $\bar{D}_w$ , and  $\bar{D}_v$  decrease as the composition changes from E<sub>30</sub> to E<sub>70</sub>. This is due to the high

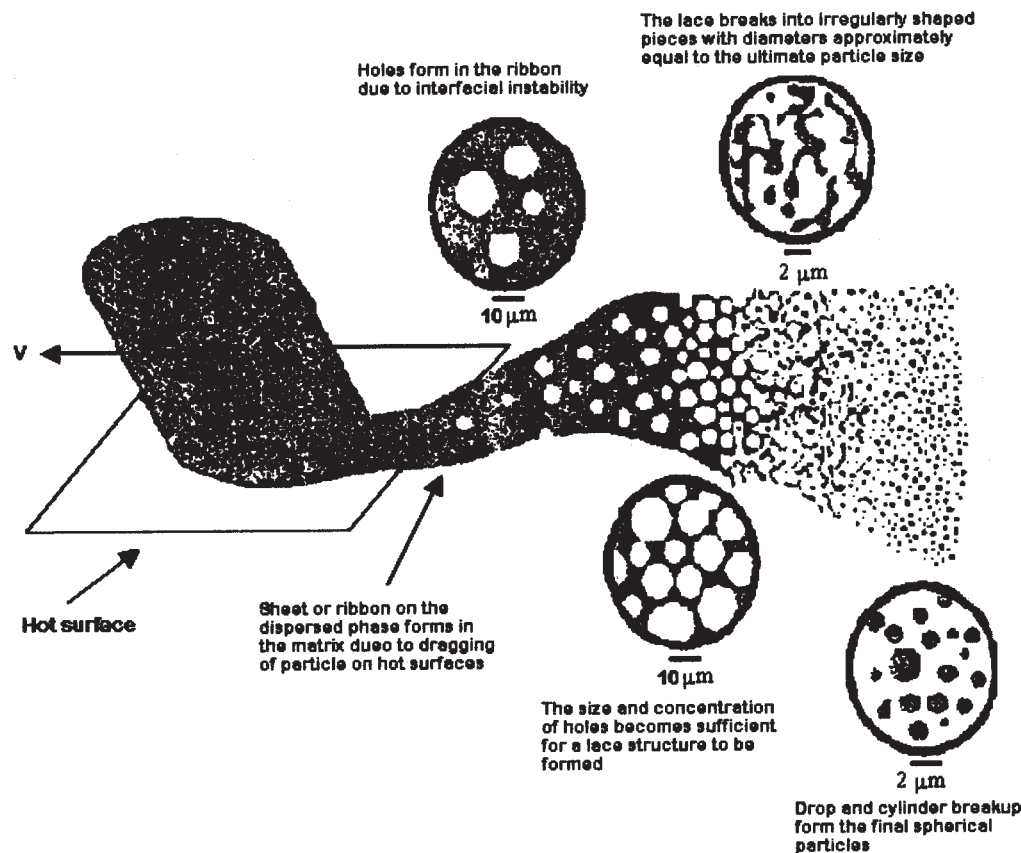


Figure 3 Schematic model of morphology development in polymer blends.

viscosity of the ENR phase compared to the NBR phase. For blends with the same processing history, the morphology is determined by the melt-viscosity ratio and composition. When the mixed polymers have similar melt viscosities, the resultant morphology will be a uniform distribution of the minor phase in the major one, no matter which is the minor component. When the components have different melt viscosities, the morphology of the resultant blend depends on whether the minor component has a lower viscosity or a higher viscosity than that of the major one. If the minor component has a lower viscosity, this component will be finely dispersed. On the other hand, the minor component will be coarsely dispersed in essentially spherical domains if its viscosity is higher than that of the major one. E<sub>50</sub> composition

shows a cocontinuous morphology. The PDI values show more uniform particle distribution for E<sub>30</sub>. The particle size distribution curve (Figure 4) is drawn by measuring 300 particles from the SEM photomicrographs. The E<sub>70</sub> composition exhibits a broader distribution curve than the E<sub>30</sub> composition.

#### Dynamic mechanical analysis of the blends

The loss tangent ( $\tan \delta$ ) values of the component polymers and the blends at 10 Hz as a function of temperature ( $-70$  to  $30^\circ\text{C}$ ) are shown in Figure 5. The glass transition temperature of NBR is at  $-9^\circ\text{C}$  and that of ENR is at  $+6^\circ\text{C}$ . In the case of blends, there is a single, sharp transition in between the  $T_g$ s of the component polymers and shifts slightly toward the high temperature region with blend ratio. This is attributed to the enhanced phase mixing between ENR and NBR. Since the  $T_g$ s of the component polymers are close ( $< 20^\circ\text{C}$ ), miscibility cannot be judged from  $T_g$  measurements. Morphology studies clearly indicate that the system is phase separated. Figure 6 shows the dependence of  $\tan \delta_{\max}$  on the weight percentage of ENR in the blend. It is observed that the damping properties of the blend increase with increasing ENR content except the slight decrease in  $\tan \delta_{\max}$  for the E<sub>30</sub> blend. The sharp

TABLE IV  
Blend Characteristics of NBR/ENR

Characteristics	E <sub>30</sub>	E <sub>70</sub>
$\bar{D}_n$ ( $\mu\text{m}$ )	1.99	1.48
$\bar{D}_w$ ( $\mu\text{m}$ )	2.90	2.53
$\bar{D}_a$ ( $\mu\text{m}$ )	2.24	2.07
$\bar{D}_v$ ( $\mu\text{m}$ )	2.60	2.44
PDI	1.27	1.96

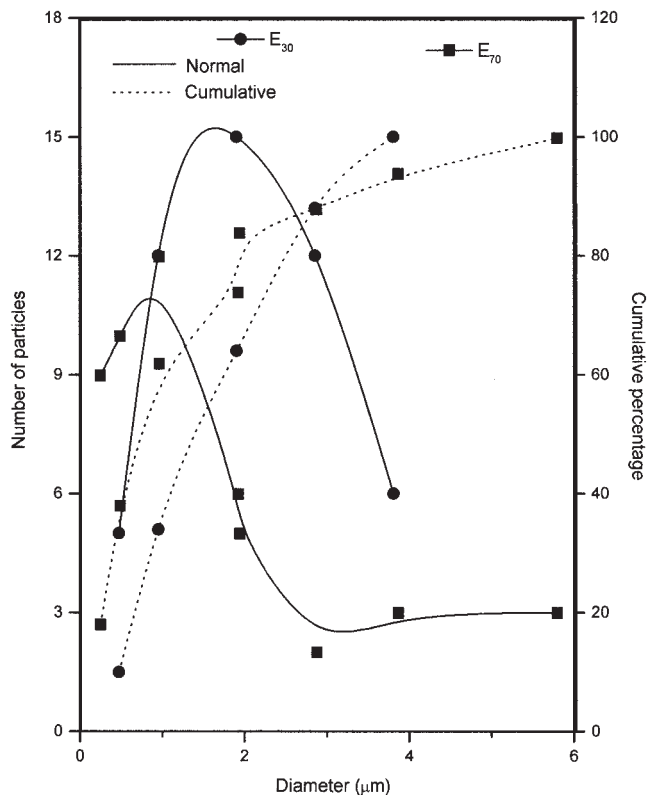


Figure 4 The particle size distribution curve of NBR/ENR blends.

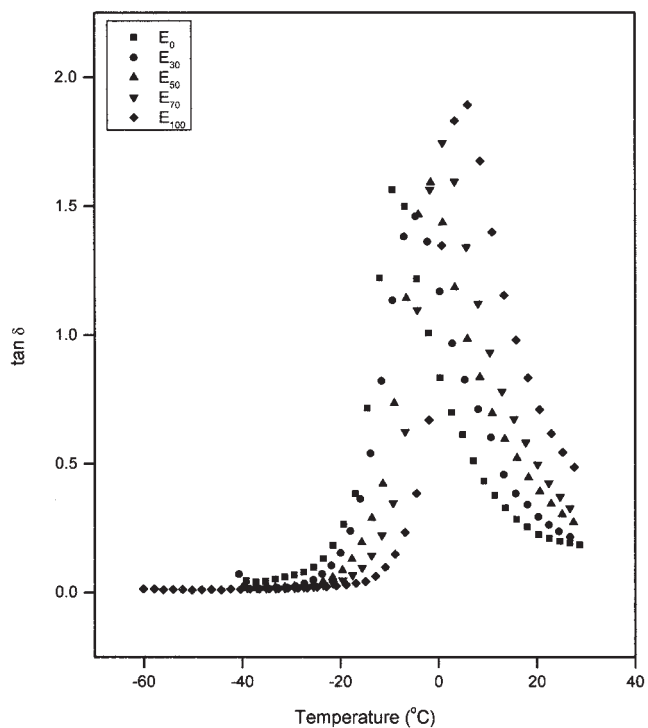


Figure 5 Effect of temperature on the tan  $\delta$  values of NBR/ENR blends at 10 Hz.

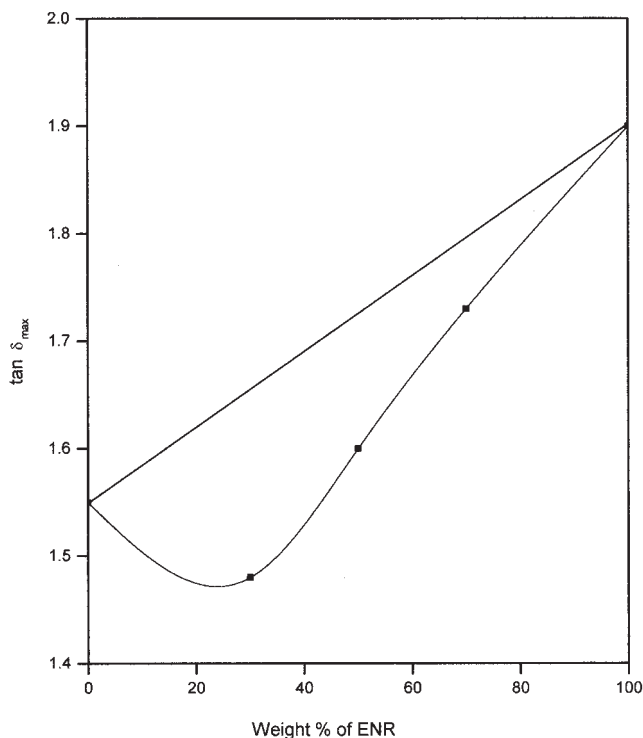


Figure 6 Variation of  $\tan \delta_{\max}$  with weight percentage of ENR.

increase in  $\tan \delta$  beyond 30% ENR is due to the continuous nature of ENR phase beyond 30% of its concentration. The effect of blend composition on the viscoelastic properties of NBR/ENR blends is given in Table V. The  $T_g$ s of the blends are between those of the pure components. The relative peak height and peak width at half height of the  $\tan \delta$  curve is measured and also given in Table V. The peak heights of the blends are lower than individual components except  $E_{70}$ . The relative peak width at half height of the blends is higher than individual components, i.e., some broadening of the glass transition zone with respect to blend composition is observed. This is clear from Figure 7. The curve shows a positive deviation depending on the composition. This indicates strong interaction between the components. Since NBR and ENR are polar, strong polar-polar interaction is possible.

The effect of temperature on the storage modulus of the blends is shown in Figure 8. The curves for all the compositions have three distinct regions: a glassy region, a transition region, and a rubbery region. Up to the glass transition temperature of NBR both phases are in the glassy state and the modulus is high. In the glassy region all the blends exhibit nearly the same moduli. Around  $-9^\circ\text{C}$  NBR becomes rubbery, but the moduli of the blends are retained due to the glassy nature of ENR. Around  $6^\circ\text{C}$  ENR also becomes rubbery. As the ENR content increases the curves get shifted to the positive side. The moduli of the blends

TABLE V  
Viscoelastic Properties of NBR/ENR Blends

Sample	tan $\delta$ peak			$T_g$ ( $^{\circ}\text{C}$ )	
	tan $\delta_{\text{max}}$	Relative peak height	Relative peak width at half height	From tan $\delta_{\text{max}}$	From $E''$ peak
E <sub>0</sub>	1.65	12.0	2.7	-4.77	-14.85
E <sub>30</sub>	1.51	11.0	3.0	0.01	-11.96
E <sub>50</sub>	1.61	11.8	3.1	2.97	-9.30
E <sub>70</sub>	1.75	12.7	3.0	5.28	-4.63
E <sub>100</sub>	1.86	13.5	2.9	10.60	0.31

increase with increase in concentration of ENR. Interestingly, the E<sub>30</sub> and E<sub>50</sub> blend curves coincide in the transition region. The loss modulus ( $E''$ ) against temperature is plotted in Figure 9. A similar behavior as in the case of the storage modulus curve is observed for the E<sub>30</sub> and E<sub>50</sub> blends. The  $T_g$  values obtained from  $E''$  versus temperature plots are always lower than those obtained from tan  $\delta_{\text{max}}$  values (Table V).<sup>14</sup>

The dynamic mechanical properties of NBR/ENR blends were analyzed from  $-70$  to  $30^{\circ}\text{C}$  at different frequencies (0.1, 1, 10, 50, and 100 Hz). Figure 10 exhibits the effect of frequency on the tan  $\delta$  values of E<sub>50</sub> composition. The tan  $\delta$  peak is shifted toward the higher temperature region with increasing frequency. Table VI shows the variation of tan  $\delta_{\text{max}}$  values with blend composition and frequency. The tan  $\delta_{\text{max}}$  values increase with the increase in frequency in all the blend

compositions except in E<sub>100</sub>. The effect of blend composition and frequency on the  $T_g$  values from the tan  $\delta$  peak is shown in Table VII. The  $T_g$  values increase with increase in frequency. This is also evident from Figure 11 in which the glass transition temperature of E<sub>50</sub> is plotted against frequency. The viscoelastic properties of a material are dependent on time, temperature, and frequency. If a material is subjected to a constant stress, its elastic modulus will decrease over a period of time. This is due to the fact that the material undergoes molecular rearrangement in an attempt to minimize the localized stress. Modulus measurements performed over a short time (high frequency) result thus in higher values, whereas measurements taken over long periods of time (low frequency) result in lower values.

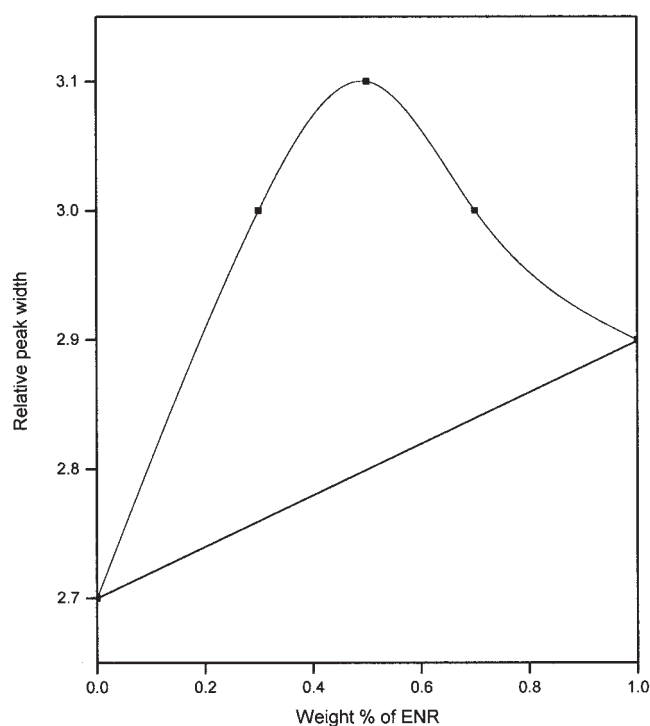


Figure 7 Effect of blend composition on the relative tan  $\delta$  peak width.

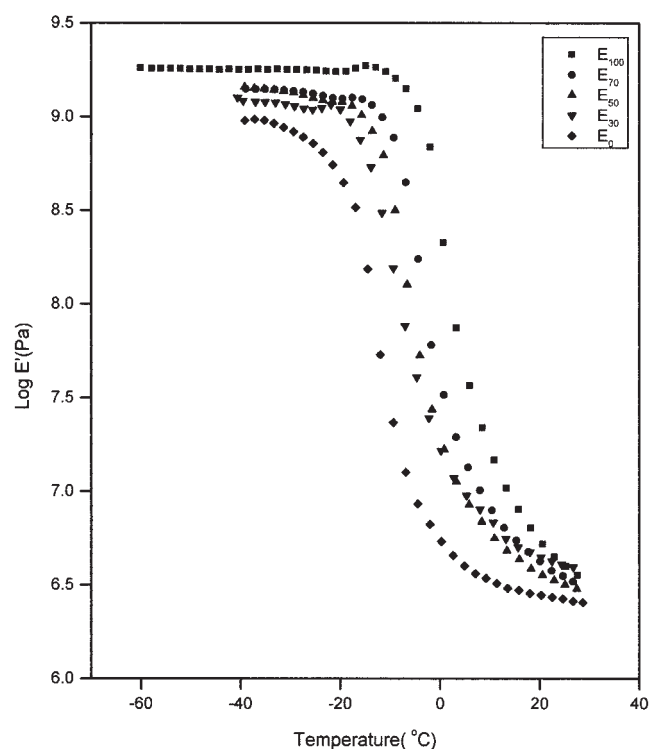


Figure 8 Effect of temperature on the storage modulus of NBR/ENR blends.

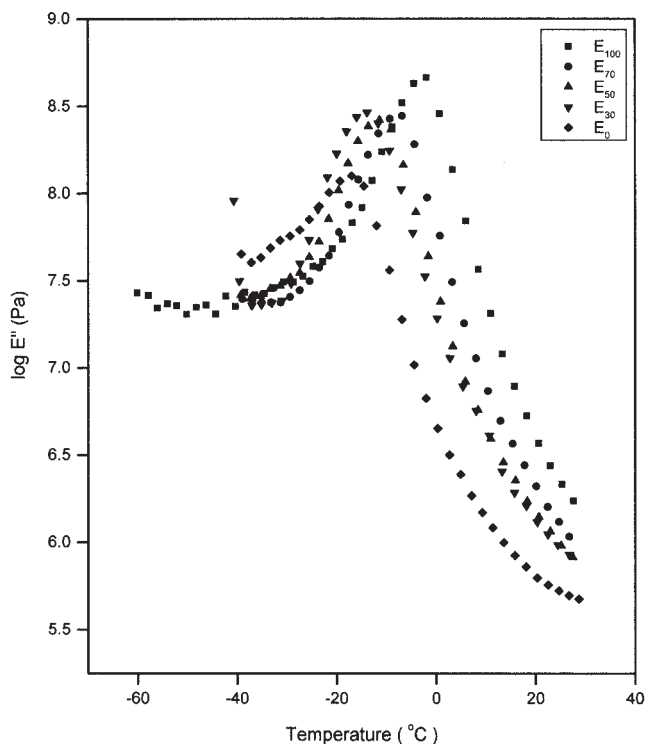


Figure 9 Effect of temperature on the loss modulus of NBR/ENR blends.

The apparent activation energy,  $E$ , for the glass transition of the blends can be calculated from the Arrhenius equation<sup>23,24</sup>

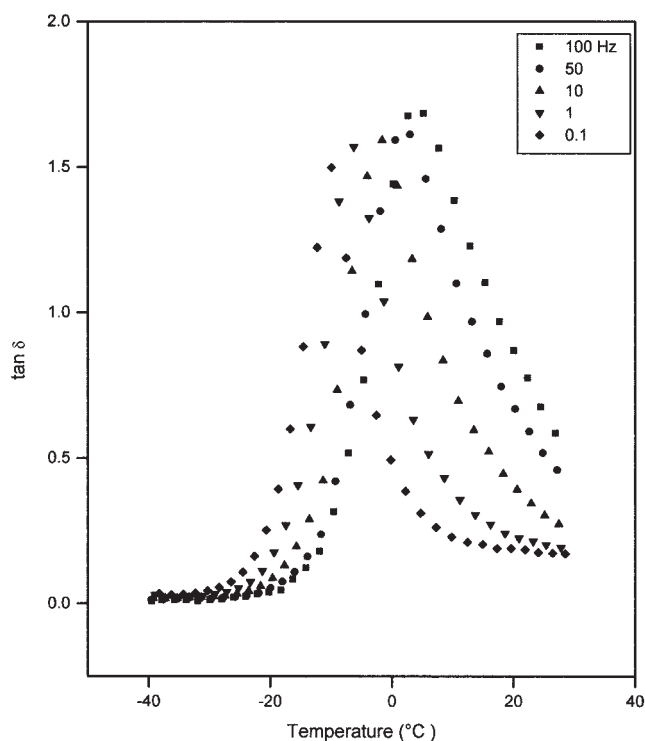


Figure 10 The variation in  $\tan \delta$  values of  $E_{50}$  at different frequencies as a function of temperature.

TABLE VI  
Effect of Blend Composition and Frequency  
on the  $\tan \delta_{\max}$  Values

Frequency (Hz)	Blend composition				
	$E_0$	$E_{30}$	$E_{50}$	$E_{70}$	$E_{100}$
100.0	1.76	1.55	1.68	1.83	1.89
50.0	1.65	1.51	1.61	1.75	1.86
10.0	1.56	1.46	1.59	1.74	1.89
1.0	1.50	1.40	1.57	1.78	1.95
0.1	1.44	1.34	1.50	1.74	1.96

$$f = f_0 \exp(-E/RT) \quad (7)$$

where  $f$  is the measuring frequency,  $f_0$  is the frequency when  $T$  approaches infinity, and  $T$  is the temperature corresponding to the maximum of loss modulus  $E''$  curve. The activation energy values obtained are given in Table VIII. The activation energy for the glass transition decreases with the increase in ENR content. This shows that more energy is required for the glass transition from the glassy to the rubbery region for NBR and NBR-rich blends.

The integral of the loss modulus versus temperature curve is characterized to develop a relationship between the extent of damping and the contribution for each group toward the damping performance. Fay et al.<sup>25</sup> suggested five methods, namely,  $\tan \delta = 0.03$ , straight line, height  $\times$  width, integral area, and constant  $E''$  for the evaluation of the area under the linear loss modulus versus temperature curve (LA).<sup>25</sup> Comparatively, the integral method includes the area under the loss modulus versus temperature curves over a well-defined temperature range without neglecting any area directly beneath the  $E''$  transition. Hence, in this system the integral method is used. The area under the linear loss modulus-temperature curve can be derived via a phenomenological treatment.<sup>26</sup>

$$LA = \int_{T_G}^{T_R} E'' dT \cong (E'_G - E'_R) \frac{R}{(E_a)_{\text{avg}}} \frac{\pi}{2} T_g^2 \quad (8)$$

TABLE VII  
Effect of Blend Composition and Frequency  
on the  $T_g$  (°C) Values from  $\tan \delta$  Peak

Frequency (Hz)	Blend composition				
	$E_0$	$E_{30}$	$E_{50}$	$E_{70}$	$E_{100}$
100.0	-2.67	2.19	5.17	7.40	10.29
50.0	-4.77	0.01	2.97	5.28	10.60
10.0	-9.38	-4.68	-1.60	0.79	5.95
1.0	-11.76	-11.37	-6.28	-4.03	0.92
0.1	-15.56	-14.83	-9.97	-7.85	-2.96



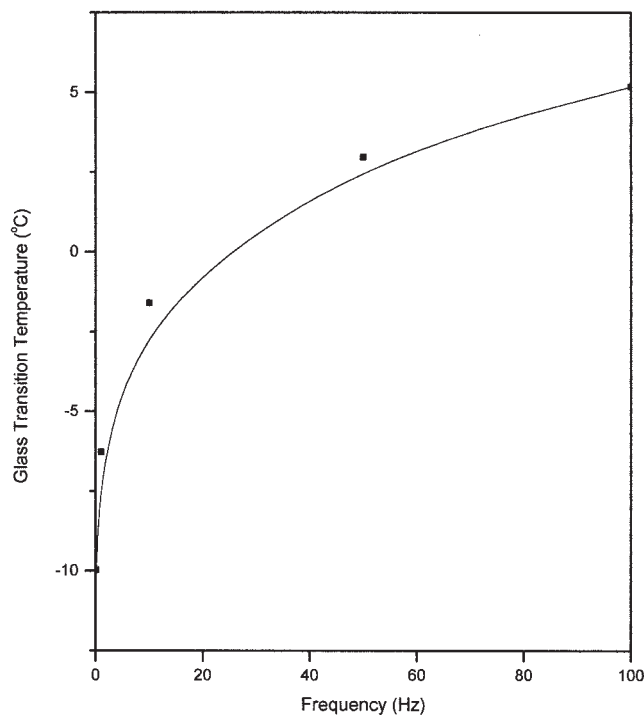


**Figure 11** Effect of frequency on the glass transition temperature of E<sub>50</sub>.

where  $E'_G$  and  $E'_R$  represent the storage moduli in the glassy and rubbery states, respectively,  $T_G$  and  $T_R$  are glassy and rubbery temperatures just below and just above the glass transition,  $(E_a)_{avg}$  is the average activation energy of the relaxation process, and  $R$  is the gas constant.

By examining the area under the glass transition, a quantitative analysis of group contributions can also be made. The group contribution analysis for LA is based on the assumption that the structural groups in the repeating units provide a weight fraction additive contribution to the total loss area. The basic equation for the group contribution analysis of LA is<sup>26,27</sup>

$$LA = \sum_{i=1}^n \frac{(LA)_i M_i}{M} = \sum_{i=1}^n \frac{G_i}{M} \quad (9)$$

where  $M_i$  is the molecular weight of the  $i^{\text{th}}$  group in the repeating unit,  $M$  is the molecular weight of the

**TABLE VIII**  
Activation Energy of NBR/ENR Blends

Sample code	$\Delta E$ (kJ/mol)
E <sub>0</sub>	377.37
E <sub>30</sub>	310.05
E <sub>50</sub>	314.92
E <sub>70</sub>	299.14
E <sub>100</sub>	276.67

**TABLE IX**  
Values of Loss Area (LA) Obtained by Integral Method and Group Contribution Analysis and Values of Crosslink Density ( $\nu$ )

Sample	Integral method (LA $\times 10^{12}$ Pa.K)	Group contribution analysis (LA $\times 10^{10}$ Pa.K)	Crosslink density ( $\nu \times 10^{-5}$ gmol/cm <sup>3</sup> )
E <sub>30</sub>	3.62	3.45	1.06
E <sub>50</sub>	3.38	3.52	1.24
E <sub>70</sub>	3.58	3.59	1.36

whole mer,  $G_i$  is the molar loss constant for the  $i^{\text{th}}$  group,  $(LA)_i$  is the loss area contributed by the  $i^{\text{th}}$  group, and  $n$  represents the number of moieties in the mer. Equation (8) provides a predictive method for LA values via the structure of the polymer.

The values of LA determined by the integral method and the predictive group contribution analysis for different blend compositions are given in Table IX. The values obtained by the integral method are larger than those obtained by group contribution analysis. The experimental values of LA are influenced by the morphology, crosslink density, and interaction between the polymer components and phase continuity. The higher values of LA indicate strong polar-polar interaction between nitrile rubber and epoxidized natural rubber. The crosslink densities of the samples were determined from the storage modulus using the equation

$$\nu = \frac{E}{6RT} \quad (10)$$

where  $E$  is the storage modulus at the plateau region of the curve,  $R$  is the universal gas constant, and  $T$  is the absolute temperature. The values of the crosslink density are also included in Table IX. It was found that the values of the crosslink density of NBR/ENR blends are between those of pure components and increase with an increase in ENR content.

### Model fitting

Various composite models such as parallel, series, Halpin-Tsai, and Kerner were used to predict the viscoelastic behavior of the blends.

The parallel model (highest-upper-bound model) is given by the equation<sup>28</sup>

$$M = M_1\phi_1 + M_2\phi_2 \quad (11)$$

where  $M$  is the property of the blend and  $M_1$  and  $M_2$  are the properties of the components 1 and 2, respectively, and  $\phi_1$  and  $\phi_2$  are the volume fractions of the components 1 and 2, respectively. In this model the

components are considered to be arranged parallel to one another so that the applied stress elongates each of the components by the same amount.

In the lowest-lower-bound series model the components are arranged in series with the applied stress. The equation is<sup>28</sup>

$$1/M = \phi_1/M_1 + \phi_2/M_2 \quad (12)$$

According to the Halpin-Tsai equation<sup>29</sup>

$$M_1/M = \frac{(1 + AiBi\phi_2)}{(1 - Bi\phi_2)} \quad (13)$$

$$Bi = \left(\frac{M_1}{M_2} - 1\right) / \left(\frac{M_1}{M_2} + Ai\right) \quad (14)$$

In this equation the subscripts 1 and 2 refer to the continuous and dispersed phases, respectively. The constant *Ai* is defined by the morphology of the system. For dispersed elastomer domains, *Ai* = 0.66.

According to the Kerner model<sup>30</sup>

$$E_b = E_m \left[ \frac{\phi_d E_d / [(7 - 5\nu_m)E_m + (8 - 10\nu_m)E_d] + \phi_m / 15(1 - \nu_m)}{\phi_d E_m / [(7 - 5\nu_m)E_m + (8 - 10\nu_m)E_d] + \phi_m / 15(1 - \nu_m)} \right] \quad (15)$$

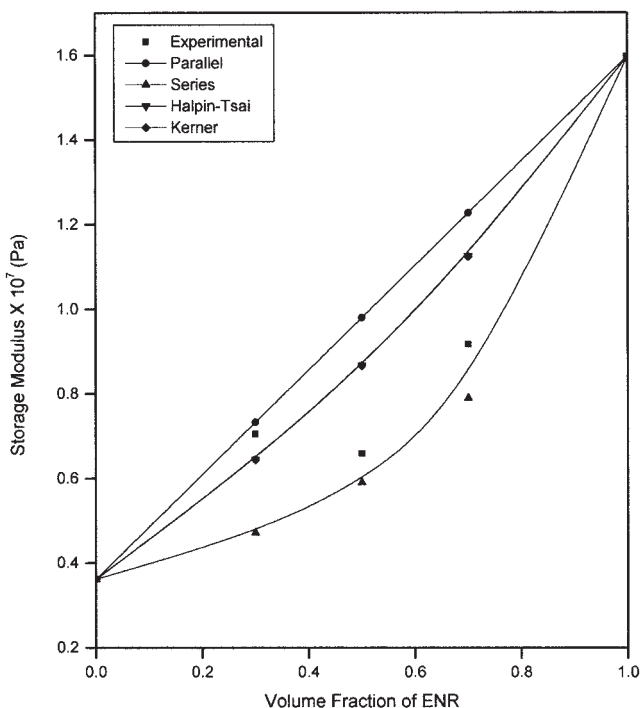


Figure 12 Applicability of various theoretical models to predict the storage modulus of NBR/ENR blends.

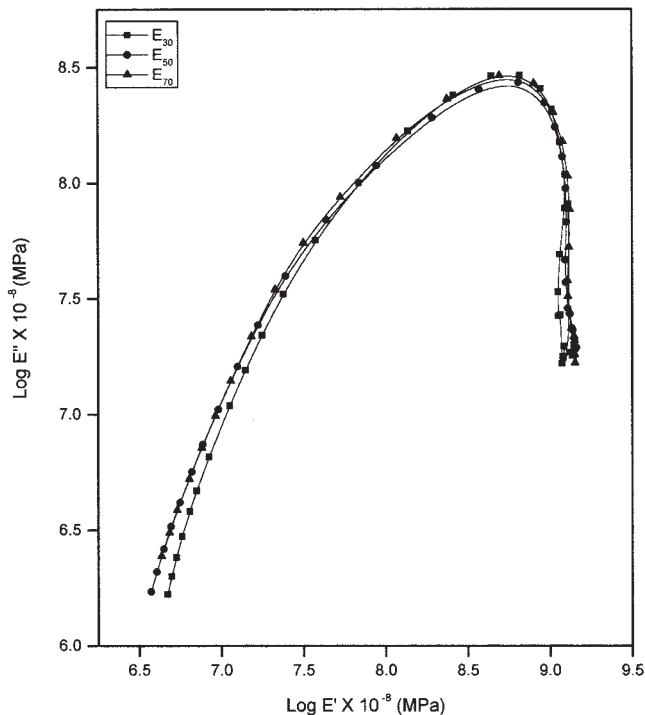


Figure 13 Cole-Cole plots of  $E_{30}$ ,  $E_{50}$ , and  $E_{70}$ .

where  $E_b$  is the blend property,  $\nu_m$  is the Poisson's ratio, and  $\phi$  is the volume fraction. The subscripts m, d, and b stand for the matrix, dispersed phase, and blend, respectively.

The model fitting for the storage modulus of NBR/ENR blends at 50 Hz and 15°C is presented in Figure 12. It is found that the experimental value for the  $E_{30}$  blend lies close to the parallel model and that for the  $E_{50}$  and  $E_{70}$  blends the experimental values come close to the series model.

### Cole-Cole analysis

The Cole-Cole plots were drawn by plotting the loss modulus ( $E''$ ) against the storage modulus ( $E'$ ). Generally homogeneous polymeric systems exhibit a semi-circle diagram.<sup>31</sup> Cole-Cole plots of miscible blends of poly(vinyl chloride) (PVC) and poly( $\alpha$ -methyl- $\alpha$ -*n*-propyl- $\beta$ -propiolactone) (PMPPL) show that this mixture does not exhibit microscale heterogeneity.<sup>23</sup> Figure 13 represents the Cole-Cole plots of  $E_{30}$ ,  $E_{50}$ , and  $E_{70}$ . The blends do not show a perfect semicircle, indicating heterogeneity in the system.

### Time-temperature superposition analysis

In polymeric systems modulus is a function of time as well as temperature. Due to the broad time dependence involved, it is not feasible to directly measure the complete behavior of the modulus as a function of

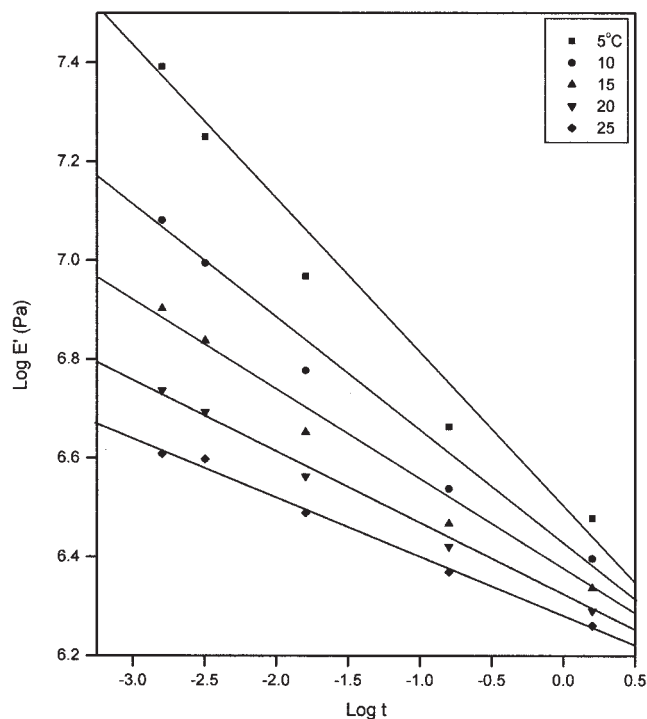


Figure 14 Log  $E'$  versus log  $t$  of NBR/ENR blends.

time at constant temperature. In principle, the complete modulus versus time behavior of any polymer at any temperature can be measured. This is achieved by a shifting procedure that enables one to construct a "master curve," which is based on the principle of time-temperature correspondence.<sup>32</sup> The master curve thus obtained is identical to that which would be measured at long times at a particular temperature.

The viscoelastic properties at a given frequency,  $f$ , are quantitatively equivalent to those of an experiment carried out over a time  $t = 1/2\pi f$ . Viscoelastic data collected at one given temperature can be superimposed upon data collected at different temperatures by shifting the curves, i.e., by using the time-temperature superposition principle. The experimental log  $E'$  versus log time graph at different temperatures is shown in Figure 14. The modulus curve at a particular temperature is then shifted along the time axis until it overlaps with the next curve. The distance between curves gives the value of the shift factor,  $a_T$ . The shift factor characterizes the rate of relaxation mechanism at some temperature  $T_i$  in comparison with the rate at a higher temperature  $T_{i+1}$ . In this way log  $a_T$  values for all temperatures were determined. The master curve was constructed by plotting log  $(t/a_T)$  versus log  $(ET_0/T)$ , where  $E$  is the storage modulus at a particular temperature,  $T_0$  is the reference temperature on the Kelvin scale, and  $T$  is the temperature of the experiment. The temperature of 15°C is taken as the reference temperature in constructing the master curve. Figure 15 shows the master curve for  $E_{50}$ . The main

advantage of the master curve is that it provides the modulus of the blend over a wide range of reduced time.

### Mechanical properties

Since these blends find extensive applications in the transport of liquids, the mechanical properties in the swollen and unswollen state has been analyzed. The stress-strain curves of the samples are shown in Figure 16. The difference in deformation characteristics of homopolymers and blends under an applied load are evident from the stress-strain curves. All the curves show typical elastomeric behavior. It can be understood from the figure that at a low strain level,  $E_0$  has the minimum stress while  $E_{100}$  has the maximum. The blend compositions occupy intermediate positions. The stress required to deform the sample increased with the increase in ENR content. This is due to the strain-induced crystallization behavior of ENR.

Stress-strain curves of samples after reaching equilibrium swelling in toluene (Figure 17) reveal that there is only a slight difference in the nature of stress-strain behavior even after reaching equilibrium. The stress at low strain follows the same pattern as that of unswollen samples. However, the strength decreases substantially as a result of swelling.

The mechanical data of homopolymers and blends are presented in Table 10. The tensile strength is max-

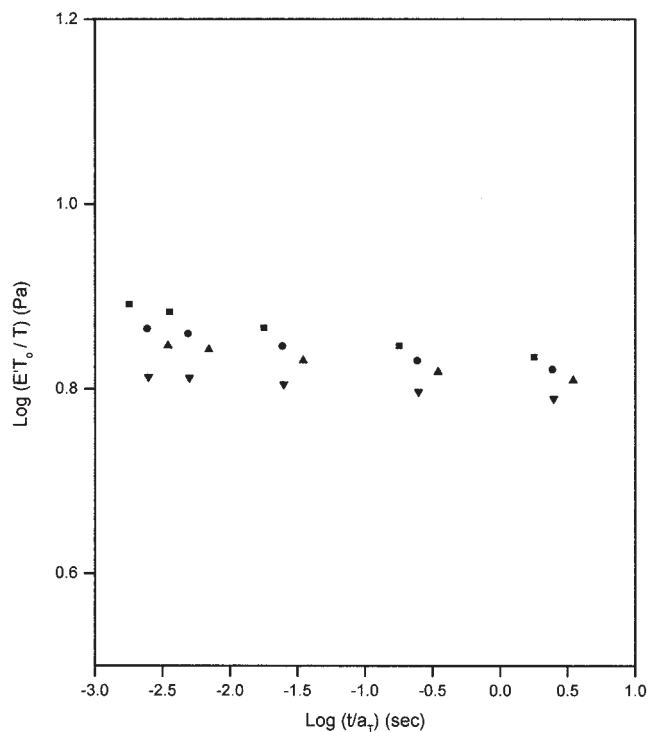
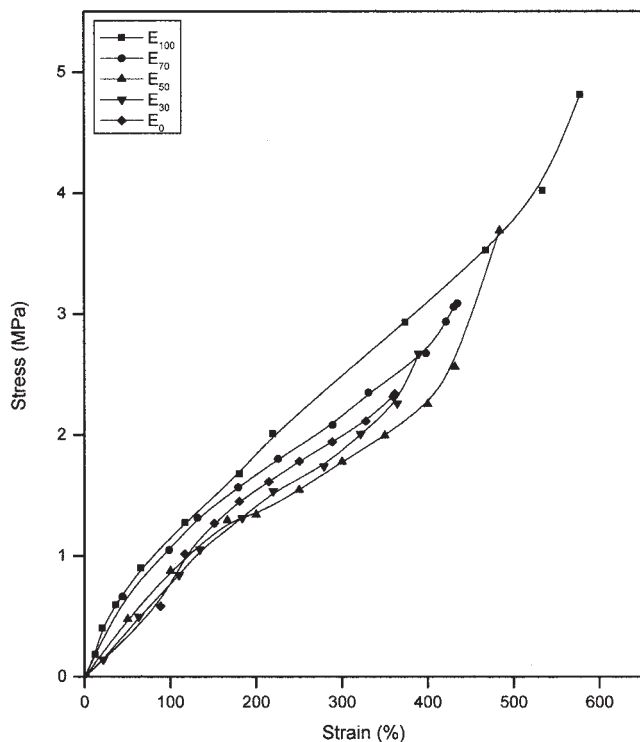


Figure 15 Plot of log  $(t/a_T)$  versus log  $(ET_0/T)$



**Figure 16** Stress-strain curves of NBR/ENR blend with different compositions in unswollen state.

imum for  $E_{100}$  due to its strain crystallization behavior and minimum for  $E_0$ . The tensile strength of the blends lies between that of pure components and, among the blends,  $E_{50}$  shows the highest strength. This behavior is due to the co-continuous morphology of  $E_{50}$ . The elongation at break is maximum for  $E_{100}$  and minimum for  $E_0$ . The Young's modulus reflects the stress behavior at low strain while the secant modulus values represent the behavior at high strain. A higher Young's modulus value for ENR compared to NBR suggests that the initial stretching of ENR requires higher stress. In the swollen state all the mechanical properties are found to be inferior to the unswollen state. In the equilibrium-swollen state, the rubber-solvent interaction is maximum while the rubber-rubber interaction is minimum and there is a total change in the conformation of polymer segments and chain entanglements. Hence the sharp decrease of mechanical properties of swollen samples is observed.

### CONCLUSION

The morphology, mechanical, and viscoelastic properties of nitrile rubber and epoxidized natural rubber blends have been established. The blend is found to be heterogeneous from the SEM micrographs. NBR/ENR 50/50 composition ( $E_{50}$ ) shows a cocontinuous morphology. The enhanced phase mixing between ENR and NBR is evident from the dynamic mechanical

analysis. The damping properties of the blends increase with increasing ENR content except in the NBR/ENR 70/30 composition. The modulus curves for all the blend compositions show three distinct regions: a glassy region, a transition region, and a rubbery region.

The damping characteristics of the blends are not much affected by the variations in frequency. The apparent activation energy for the transition decreases with the increase in weight percentage of ENR. The values of loss area under the linear loss modulus-temperature curve (LA) estimated by the integral method are larger than that determined quantitatively by the group contribution analysis, suggesting strong polar-polar interaction between nitrile rubber and epoxidized natural rubber. Applicability of various theoretical models to predict the storage modulus of the blends was checked and it was found that the experimental values of NBR/ENR 70/30 composition lie close to the parallel model while those of the NBR/ENR 50/50 and NBR/ENR 30/70 compositions lie close to the series model. The homogeneity of the system is further studied by Cole-Cole analysis. A master curve was constructed for the storage modulus of the NBR/ENR 50/50 composition based on the time-temperature superposition principle.

The deformation characteristics of NBR/ENR blends are clear from the stress-strain curves. The tensile strength and elongation at break are maximum

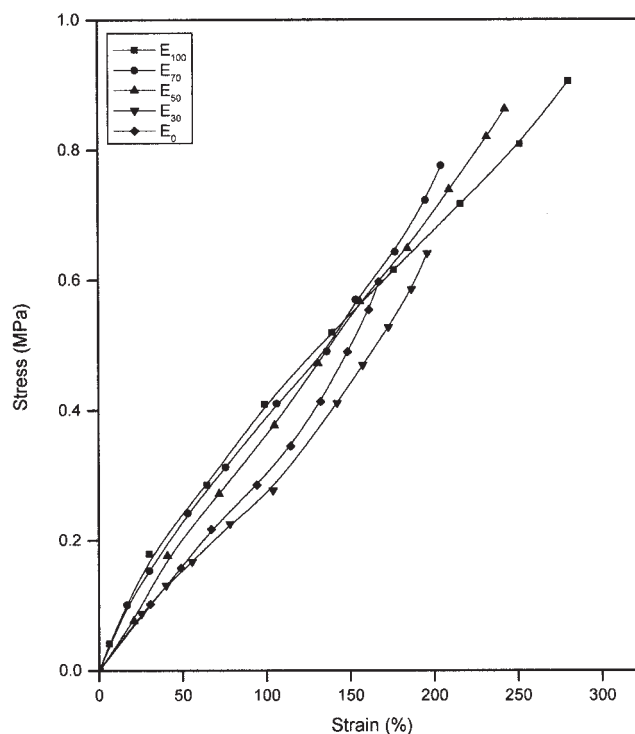


**Figure 17** Stress-strain curves of NBR/ENR blend with different compositions in swollen state.

**TABLE X**  
**Mechanical Properties of NBR/ENR Blends**

Sample	System	Tensile strength (MPa)	E.B. %	Young's modulus (MPa)	Secant modulus (MPa)		
					$M_{100}$	$M_{200}$	$M_{300}$
Unswollen	E <sub>100</sub>	4.81	578	16.24	0.76	1.55	1.99
	E <sub>70</sub>	3.09	435	14.67	0.79	1.41	1.86
	E <sub>50</sub>	3.69	484	9.71	0.88	1.34	1.76
	E <sub>30</sub>	2.67	390	7.50	1.05	1.67	2.15
	E <sub>0</sub>	2.34	362	6.61	1.15	1.84	2.49
	E <sub>100</sub>	0.99	295	7.77	0.41	0.68	0.99
Swollen	E <sub>70</sub>	0.78	205	5.80	0.39	0.75	—
	E <sub>50</sub>	0.86	237	3.93	0.36	0.71	—
	E <sub>30</sub>	0.64	196	3.49	0.28	—	—
	E <sub>0</sub>	0.59	167	3.79	0.30	—	—

for pure ENR due to its strain crystallization behavior and minimum for NBR. The tensile strength of the blends lies between that of pure components. Among the blends the NBR/ENR 50/50 composition shows the highest strength due to its cocontinuous morphology. In the swollen state, there is an overall reduction in the magnitude of these properties. Further experiments are in progress on the applicability of these membranes.

A.E.M. is grateful to the Council of Scientific and Industrial Research for the award of Senior Research Fellowship and to Dr. Zacharia Oommen of C.M.S. College, Kottayam for his help in the morphological studies.

## References

- Paul, D. R.; Newman, S. In *Polymer Blends*, Vol. I; Academic Press: New York, 1978; p 1.
- Smith, R. W.; Andries, J. C. *Rubber Chem Technol* 1974, 47, 64.
- Dao, K. C. *Polymer* 1984, 25, 1527.
- Cimmino, S.; D'orazio, L.; Greco, R.; Maglio, G.; Malinconico, M.; Mancarella, C.; Martuscelli, E.; Palumbo, R.; Ragosta, G. *Polym Eng Sci* 1984, 24, 48.
- Varghese, H.; Bhagawan, S. S.; Thomas, S. *J Appl Polym Sci* 1999, 71, 2335.
- Johnson, T.; Thomas, S. *J Mater Sci* 1999, 34, 13, 3221.
- Oommen, Z.; Gopinathan Nair, M. R.; Thomas, S. *Polym Eng Sci* 1996, 36, 1.
- George, S. C.; Ninan, K. N.; Thomas, S. *J Appl Polym Sci* 2000, 78, 1280.
- Asaletha, R.; Kumaran, M. G.; Thomas, S. *Rubber Chem Technol* 1995, 68, 671.
- George, J.; Joseph, R.; Varughese, K. T.; Thomas, S. *J Appl Polym Sci* 1995, 57, 449.
- Ramesh, P.; De, S. K. *J Appl Polym Sci* 1993, 50, 1369.
- Varughese, K. T.; Nando, G. B.; De, P. P.; De, S. K. *J Mater Sci* 1988, 23, 3894.
- Patri, M.; Samui, A. B.; Deb, P. C. *J Appl Polym Sci* 1993, 48, 1709.
- Koshy, A. T.; Kuriakose, B.; Varghese, S.; Thomas, S. *Polymer* 1993, 34, 3428.
- Varghese, H.; Bhagawan, S. S.; Rao, S. S.; Thomas, S. *Eur Polym J* 1995, 31, 957.
- George, S.; Neelakantan, N. R.; Varughese K. T.; Thomas, S. *J Polym Sci Polym Phys Ed* 1997, 35, 2309.
- Oommen, Z.; Groeninckx, G.; Thomas, S. *J Polym Sci Polym Phys Ed* 2000, 38, 525.
- Bandyopadhyay, G. G.; Bhagawan, S. S.; Ninan, K. N.; Thomas, S. *J Appl Polym Sci* 1999, 72, 165.
- Gillberg, G.; Sawyer, L. C.; Promislow, A. L. *J Appl Polym Sci* 1983, 28, 3723.
- Tokita, N. *Rubber Chem Technol* 1977, 50, 293.
- Scott, C. E.; Macosko, C. W. *Polym Bull* 1991, 26, 341.
- Gorton, A. D. T.; Pendle, T. D. *NR Technol* 1981, 12, 1.
- Malik, T. M.; Prud'homme, R. E. *Polym Eng Sci* 1984, 24, 144.
- Hourston, D. J.; Huson, M. G.; McCluskey, J. A. *J Appl Polym Sci* 1986, 31, 709.
- Fay, J. J.; Thomas, D. A.; Sperling, L. H. *J Appl Polym Sci* 1991, 43, 1617.
- Chang, M. C. O.; Thomas, D. A.; Sperling, L. H. *J Appl Polym Sci* 1987, 34, 409.
- Chang, M. C. O.; Thomas, D. A.; Sperling, L. H. *J Polym Sci Polym Phys Ed* 1988, 26, 1627.
- Thomas, S.; George, A. *Eur Polym J* 1992, 28, 1451.
- Nielson, L. E. *Rheol Acta* 1974, 13, 86.
- Kerner, E. H. *Proc Phys Soc* 1956, 69B, 808.
- Cole, K. S.; Cole, R. H. *J Chem Phys* 1941, 9, 341.
- Aklonis, J. J.; MacKnight, W. J. In *Introduction to Viscoelasticity*; John Wiley and Sons: New York, 1983.